2019

Gamma Radiation and Neutron Shielding Properties of Transparent Alkali Borosilicate Glass Containing Lead

Elsayed Salama
elsayed.salama@bue.edu.eg

Abeer Maher
abeer.maher@bue.edu.eg

Gamal Youssef
Ain Shams University, gamalyoussef21@gmail.com

Journal of Physics and Chemistry of Solids 131 (2019) 139–147

Contents lists available at ScienceDirect

Journal of Physics and Chemistry of Solids

journal homepage: www.elsevier.com/locate/jpcs

Gamma radiation and neutron shielding properties of transparent alkali borosilicate glass containing lead

E. Salama[a,b,*], Abeer Maher[b], G.M. Youssef[a]

[a] Physics Department, Faculty of Science, Ain Shams University, Cairo, Egypt
[b] Basic Science Department, Faculty of Engineering, The British University in Egypt (BUE), Egypt

ARTICLE INFO

Keywords:
Borosilicate glass
Gamma ray shielding
Lead
Lithium
Neutron removal cross section

ABSTRACT

In this study, lithium sodium borosilicate glasses with chemical compositions of $xPbO\text{-}40B_2O_3{-}25Na_2O{-}5Li_2O\text{-}(30 - x)SiO_2$ (where x = 0, 5, 10, 15, 20, and 25 mol%) were prepared by using the conventional melt-quenching technique. The amorphous nature and the effects of Pb + 2 ions in the glass structure were explored by using X-ray diffraction and Fourier transform infrared spectroscopy analyses, respectively. The gamma radiation and neutron shielding properties of the glass system were investigated by determining the mass attenuation coefficients, half value layer, gamma-ray exposure build-up factor (EBF), and fast neutron removal cross section. The EBFs were calculated using the general progressive fitting parameter formula for photon energies of 0.015–15 MeV to penetration depths of 40 mfp. The effective atomic number (Z_{eff}) and electron density (N_{eff}) were determined for all of the prepared glasses. For validation purposes, the experimental values of the mass attenuation coefficient, half value layer, Z_{eff}, and N_{eff} for all of the prepared glasses at 0.239, 0.662, 0.911, and 1.332 MeV were compared with their theoretical values. The fast neutron removal cross sections of the prepared glasses ranged from 0.0890 to 0.1375 cm^{-1}, which corresponded to concentrations of 0–25 PbO mol%. The results confirmed that the glasses prepared with lead concentrations of 5–25 PbO mol% have suitable and comparable gamma attenuation coefficients for use as efficient transparent gamma ray and neutron shielding materials.

1. Introduction

The contributions of nuclear technology have substantially improved in areas such as the production of electricity in nuclear power plants, radiotherapy and diagnostics in medicine, as well as applications in agriculture and various other industries. These improvements have been achieved by harnessing radioisotopes and providing suitable protection via shielding and dosimetry. The choice of an appropriate material for shielding is influenced by the type of radiation and the application area. In reactor shielding, primary neutrons and gamma rays (generated inside the nuclear reactor core) as well as secondary gamma rays (emitted due to the interactions between neutrons and external materials in the reactor core) are the major forms of radiation that require shielding [1].

Moreover, suitable radiation transparent shielding materials are needed in radiotherapy. Thus, glass compositions have been developed with excellent transparent properties and high radiation attenuation parameters [2–4]. These qualities make them suitable candidates for use in some protective materials. Glasses have dual properties because they are transparent to visible light and they can attenuate gamma rays, thereby allowing their use as transparent radiation shields.

Concrete is the most commonly used radiation shielding material because of its cost and adaptability to any construction design, but the usage of concrete has several drawbacks due to its density and structural strength, which decreases with the water content, thereby directly affecting the calculated shielding parameters [5].

The effects of gamma irradiation and the addition of heavy metal oxides to borosilicate glasses have been investigated in previous studies [6–8]. Glasses containing heavy metal oxides are used intensively in several industrial area, such as in reflecting windows, thermal and mechanical sensors, optical and electronic devices, and gamma radiation shielding [9–17]. The addition of non-conventional glass formers such as lead oxide (PbO) has important effects by drastically changing the structure of the glass network. The Pb ion improves the resistance to diversification, increases the chemical durability, reduces the melting point, and increases the mass density, polarizability, and refractive index of the glass material [18,19]. Pb can act as either a glass network former or a modifier depending on its concentration in composite

* Corresponding author. Physics Department, Faculty of Science, Ain Shams University, Cairo, Egypt.
E-mail address: e_elsayed@sci.asu.edu.eg (E. Salama).

https://doi.org/10.1016/j.jpcs.2019.04.002
Received 15 August 2018; Received in revised form 30 March 2019; Accepted 1 April 2019
Available online 03 April 2019
0022-3697/

glasses. The addition of sodium and lithium oxide can also enhance various properties of the hosting glass. Adding sodium oxide decreases the melting point, as well as expanding the glass-forming region and facilitating ion exchange [9]. Moreover, glass systems that contain lithium oxide exhibit rapid ionic conductivity and high refraction [20].

Borosilicate glasses have further advantages such as chemical endurance and better heat stability. In addition, borosilicate glasses have very low thermal expansion coefficients and high capacities for significant visible light transmission [21–23].

In the present study, we synthesized inexpensive vitreous lithium sodium borosilicate glasses containing PbO, with possible applications in the field of radiation shielding. Radiation shielding parameters were determined comprising the mass attenuation coefficient, neutron removal cross-section, and exposure build-up factors (EBFs) at different PbO mol% levels and energies.

2. Materials and methods

A chemical system with a composition of xPbO-40B_2O_3-25 Na_2O−5Li_2O-(30 - x)SiO_2 (where x = 0, 5, 10, 15, 20, and 25 mol%) was prepared using the conventional melt-quenching technique. The mixtures of high purity chemicals comprising PbO, Si_2O, Li_2O, Na_2CO_3, and H_3BO_3 were manually ground to obtain a fine powder. The prepared powders were melted at 1100 °C in a high purity porcelain crucible until a homogenous bubble-free liquid was formed. The melts were annealed in a stainless steel mold at ~350 °C for 2 h. The samples were then manually polished to obtain maximum flatness.

The prepared glasses in their amorphous state were examined by X-ray diffraction (XRD) analysis at room temperature. XRD analysis was performed with a Philips X'pert Pro X-ray powder diffractometer (Malvern Panalytical, Almelo, Netherlands) using Cu Kα radiation (1.5418 Å) at a scanning speed of 0.3 s.

A JASCOFT-IR6200 spectrometer (JASCO, Tokyo, Japan) was used for Fourier transform infrared spectroscopy (FTIR) to obtain the absorption spectra of the prepared samples with the KBr pellet technique in the spectral range of 400–4000 cm^{-1}.

The density of the prepared glass samples was measured at room temperature using the conventional method based on the standard Archimedes principle [20] according to the following relationship:

$$\rho = \frac{W_a}{W_a - W_b}\rho_b \quad (1)$$

where W_a is the weight of the sample in air, W_b is the weight in xylene, and ρ_b is the density of xylene (ρ_b = 0.863 g/cm^3).

The total molecular weight of the multi-component glass system is given by:

$$M_T = \sum_i M_i x_i \quad (2)$$

where x_i and M_i are the mole fraction and molecular weight of the constituent oxide i, respectively. The corresponding molar volume (V_M) was determined using the following standard formula.

$$V_M = M_T/\rho \quad (3)$$

The gamma ray shielding parameters of the prepared glasses were measured at four gamma energies comprising 0.662 MeV gamma photons emitted from a Cs-137 point source, 0.239 MeV and 0.911 MeV emitted from a ^{232}Th point source, and 1.332 MeV emitted from a Co-60 point source under appropriate geometrical conditions using a NaI (Tl) scintillation detector (Teledyne Isotopes "2 × 2″ NaI (Tl) Scintillation Detector, Alabama, USA) with an energy resolution of 8% at 662 keV.

3. Theoretical background

The attenuation of a gamma-ray beam through a medium follows the modified Beer–Lambert law as follows [24]:

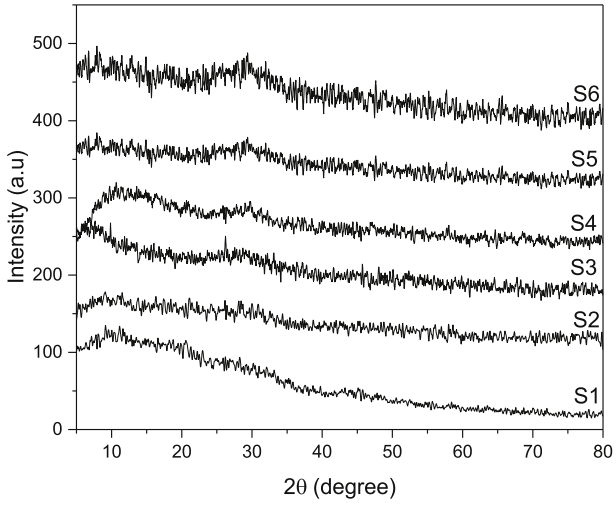

Fig. 1. X-ray diffraction patterns obtained for lithium sodium borosilicate glasses containing PbO.

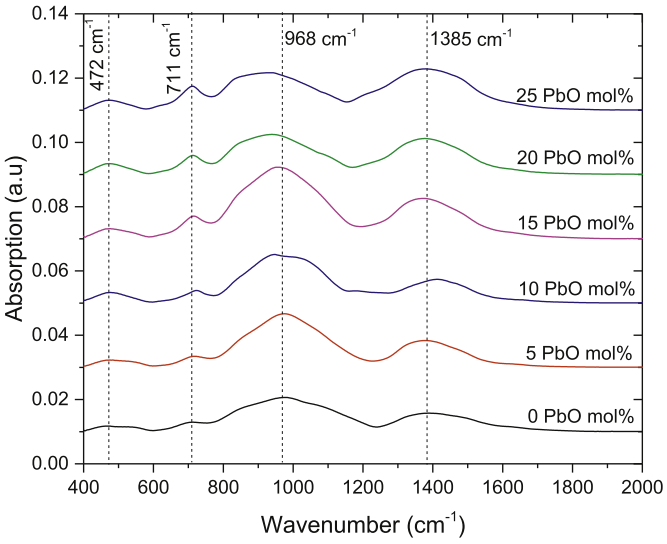

Fig. 2. Fourier transform infrared spectroscopy analysis of lithium sodium borosilicate glasses containing PbO.

$$I = B \times I_0 \times e^{-\mu x} \quad (4)$$

where I_o and I are the initial and transmitted photon intensities, respectively, μ is a linear attenuation coefficient (in cm^{-1}), and B (E, x) is the build-up factor, which depends on the energy E of the incident photon and the thickness x (cm) of the material. By using the values measured for the linear attenuation coefficient and the mass density (ρ), the mass attenuation coefficient (μ_m) can be determined by the following relationship.

$$\mu_m = \frac{\mu}{\rho} \quad (5)$$

The half value layer (HVL) of any material is defined as the thickness of a material that reduces the photon beam intensity to one half of its initial intensity, which can be calculated with the following formula:

$$HVL = \frac{0.693}{\mu} \quad (6)$$

where μ is the linear attenuation coefficient of the material. Clearly, the linear attenuation coefficient depends on the type of material as well as its mass density and beam energy.

In the case of a compound or a mixture, the mass attenuation

Table 1
Designations of infrared bands in the spectra obtained for the prepared glass samples.

Peak Position (cm^{-1})	Assignment	Reference Range
1385	Stretching relaxation of B—O bonds in trigonal BO_3 units	~1400 [35,36]
968	Stretching vibrations of B—*O*—Si linkages	950–1050 [37,38]
711	Stretching vibrations of B—*O*—B linkages in a borate network (two silicate chains and borate phases)	~700 [39,40]
472	Vibrations of the metal cations Na^+, Pb^{2+}, and Li^+	< 600 [41,42]

Table 2
Chemical compositions (mol%) of the prepared samples.

Sample Code	Composition (mol%)				
	PbO	B_2O_3	Na_2O	Li_2O	SiO_2
S0	0	40	25	5	30
S1	**5**	40	25	5	25
S2	10	40	25	5	20
S3	15	40	25	5	15
S4	20	40	25	5	10
S5	25	40	25	5	5

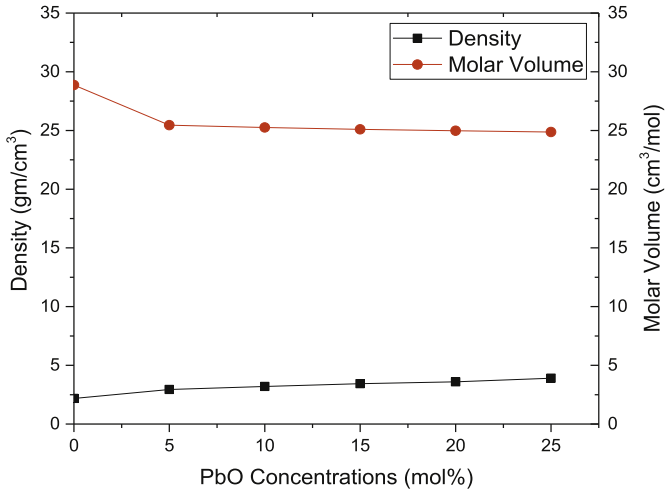

Fig. 3. Mass density and molar volume values for lithium sodium borosilicate glasses containing PbO.

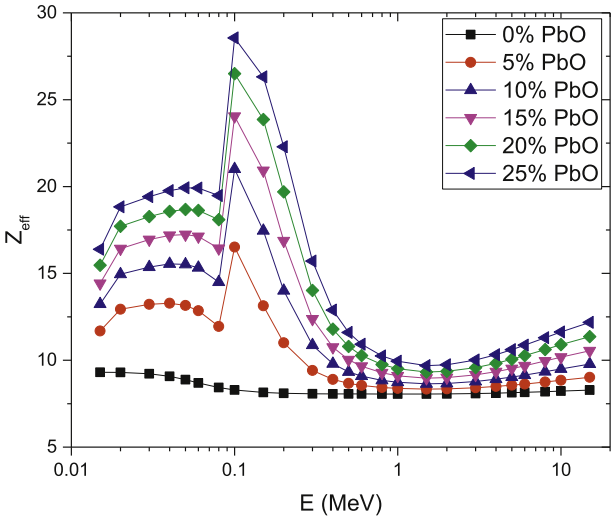

Fig. 4. Effective atomic numbers for lithium sodium borosilicate glasses containing PbO at 0.662 MeV.

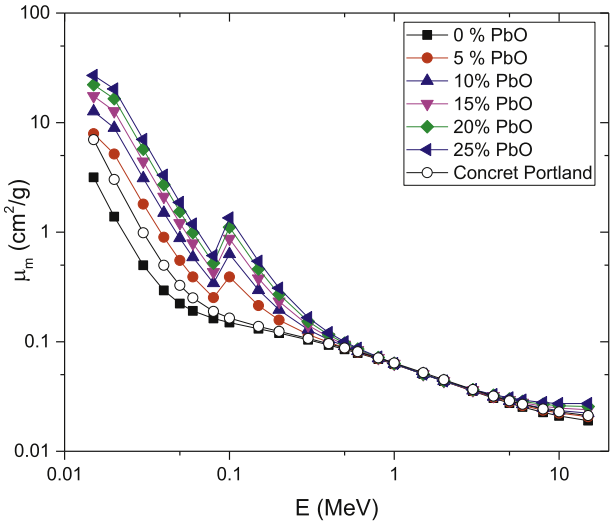

Fig. 5. Mass attenuation coefficients for lithium sodium borosilicate glasses containing PbO.

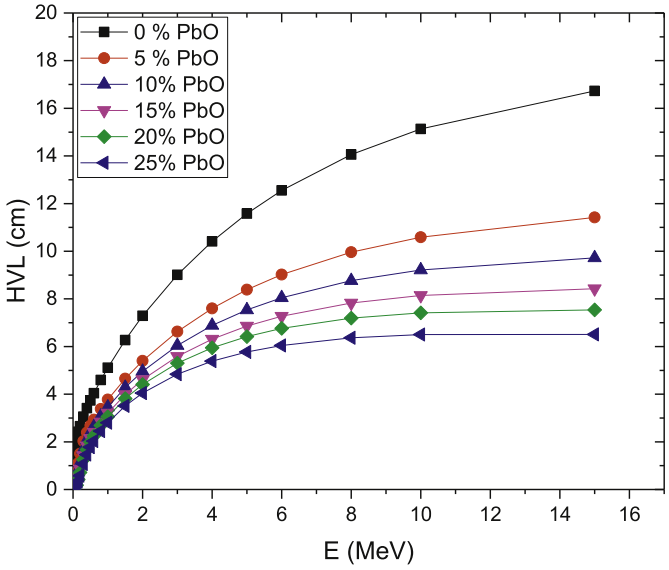

Fig. 6. Half value layer (HVL) results for lithium sodium borosilicate glasses containing PbO.

coefficient (μ_m) can be determined by:

$$\mu_m = \sum_i w_i(\mu_m)_i \tag{7}$$

where $(\mu_m)_i$ is the mass attenuation coefficient of the *i*th element of the mixture. $(\mu_m)_i$ is a function of the energy for every element. XCOM is database of photon cross sections prepared by the National Institute of Standard and Technology (NIST), which contains the attenuation coefficients of all elements in the periodic table at different energies [25]. In this study, the XCOM web database was used to calculate the values of the mass attenuation coefficients for the glasses over a wide

Table 3
Comparisons of different shielding materials at 0.662 MeV.

System	Lead concentration (mol%)	Range of μ_m (cm^2/g) × 10^{-2}	Z_{eff}	Reference
Lead sodium borate glasses ($PbO-Na_2O-B_2O_3$)	5–25	8.04–9.30	8.78–15.82	[9]
Lead borate glasses ($PbO-B_2O_3$)	30–70	8.31–9.96	9.96–21.25	[43]
Lead barium phosphate glasses ($P_2O_5-PbO-BaO$)	40–65	9.00–9.90	–	[44,45]
Barite concrete	–	6.7–7.8	–	[46,47]
Portland concrete	–	7.76		[25]
Lead sodium lithium borosilicate glasses ($PbO-Na_2O-SiO_2-B_2O_3-LiO_3$)	5–25	7.89–8.73	8.06–10.59	Current study

Table 4
Mass attenuation coefficient, Half value layer, Effective atomic number and Effective electron density for lithium sodium borosilicate glasses containing PbO at different photon energies.

Energy (MeV)	PbO mol %	μ_m (cm^2/g)		HVL (cm)		Z_{eff} (electrons/atom)		N_{eff} (electrons/g)x10^{23}	
		Theoretical	Experimental	Theoretical	Experimental	Theoretical	Experimental	Theoretical	Experimental
0.239	0.000	0.113	0.111 ± 0.004	2.818	2.868	8.091	7.946 ± 0.029	2.689	2.640
	5.000	0.136	0.135 ± 0.003	1.735	1.748	10.299	10.175 ± 0.029	2.321	2.293
	10.000	0.160	0.155 ± 0.007	1.356	1.400	12.598	12.254 ± 0.091	2.148	2.090
	15.000	0.183	0.177 ± 0.008	1.103	1.140	14.805	14.340 ± 0.088	2.031	1.967
	20.000	0.206	0.195 ± 0.015	0.937	0.990	17.104	16.187 ± 0.026	1.962	1.857
	25.000	0.229	0.227 ± 0.006	0.773	0.783	19.311	19.073 ± 0.059	1.903	1.880
0.662	0.000	0.076	0.075 ± 0.003	4.189	4.245	8.057	8.028 ± 0.025	2.677	2.668
	5.000	0.077	0.077 ± 0.002	3.065	3.065	8.492	8.480 ± 0.044	1.914	1.911
	10.000	0.078	0.079 ± 0.001	2.781	2.746	8.965	8.949 ± 0.080	1.529	1.526
	15.000	0.079	0.079 ± 0.003	2.555	2.555	9.464	9.460 ± 0.222	1.298	1.297
	20.000	0.080	0.080 ± 0.002	2.413	2.413	10.011	9.995 ± 0.034	1.148	1.146
	25.000	0.080	0.082 ± 0.004	2.218	2.164	10.587	10.580 ± 0.100	1.043	1.043
0.911	0.000	0.065	0.065 ± 0.001	4.898	4.898	8.091	8.053 ± 0.116	2.689	2.676
	5.000	0.066	0.067 ± 0.002	3.576	3.522	8.367	8.615 ± 0.096	1.886	1.942
	10.000	0.066	0.065 ± 0.001	3.287	3.338	8.735	8.638 ± 0.161	1.490	1.47
	15.000	0.066	0.063 ± 0.002	3.058	3.204	9.195	8.714 ± 0.067	1.261	1.195
	20.000	0.067	0.064 ± 0.004	2.881	3.016	9.563	9.197 ± 0.088	1.097	1.055
	25.000	0.067	0.066 ± 0.002	2.648	2.688	10.023	9.864 ± 0.078	9.879	9.723
1.332	0.000	0.054	0.052 ± 0.003	5.896	6.123	8.091	7.846 ± 0.026	2.689	2.607
	5.000	0.054	0.053 ± 0.001	4.370	4.453	8.367	8.221 ± 0.098	1.886	1.853
	10.000	0.054	0.054 ± 0.001	4.018	4.018	8.643	8.724 ± 0.172	1.474	1.488
	15.000	0.054	0.053 ± 0.002	3.738	3.808	9.011	8.886 ± 0.133	1.236	1.219
	20.000	0.054	0.054 ± 0.001	3.575	3.575	9.379	9.479 ± 0.059	1.076	1.087
	25.000	0.054	0.053 ± 0.001	3.285	3.347	9.747	9.651 ± 0.108	9.607	9.512

range of energies from 0.015 to 15 MeV.

The mean free path (mfp) values were calculated for the prepared glasses using the linear attenuation coefficient (μ) with the following equation.

$$MFP = \frac{1}{\mu} \tag{8}$$

The effective atomic number of a material (Z_{eff}) is defined as the ratio between its effective atomic cross section (σ_a) and electronic cross-section (σ_e). Using the values obtained for μ_m, the Z_{eff} values were determined for the prepared glass samples using the following relationship [26]:

$$Z_{eff} = \frac{\sigma_a}{\sigma_e} = \frac{\sum_i f_i A_i (\mu_m)_i}{\sum_i f_i \frac{A_i}{Z_i} (\mu_m)_i} \tag{9}$$

where A_i and Z_i represent the atomic weight and atomic number for the ith element, respectively, and f_i represents its fractional abundance with respect to the number of atoms. The Auto-Zeff program prepared in Visual Basic and recently introduced by Taylor [27] was employed as user-friendly software for rapidly computing the effective atomic numbers.

The effective electron density (N_{eff}) was calculated for the glasses using the following formula [28]:

$$N_{eff} = N_A \frac{Z_{eff}}{\sum_i f_i A_i} \quad (electrons/g) \tag{10}$$

where N_A is Avogadro's number, and A_i and f_i are the atomic mass and molar fraction of the ith element in the glass sample, respectively. Equation (10) shows that N_{eff} varies with the energy in a similar manner to Z_{eff} depending on the interaction processes involved.

The equivalent atomic number (Z_{eq}) was calculated for the prepared glass samples by matching $R = (\mu_m)_{comp}/(\mu_m)_{total}$ at a given energy with the ratios R_1 and R_2 for two pure elements at the same energy such that R was between the two ratios R_1 and R_2 (adjacent to R). Hence, the two elements had two successive atomic numbers Z_1 and Z_2, and the value of Z_{eq} could be interpolated using the following logarithmic interpolation formula [29].

$$Z_{eq} = \frac{Z_1(\log R_2 - \log R) + Z_2(\log R - \log R_1)}{\log R_2 - \log R_1} \tag{11}$$

The EBF values were calculated for the prepared glasses by general progressive (G-P) interpolation in the gamma ray energy range of 0.015–15 MeV up to 40 mfp using the following equations [30,31] according to Harima et al. (1993):

$$B(E, X) = 1 + \frac{b-1}{K-1}(K^x - 1) \quad \text{for } K \neq 1 \tag{12}$$

$$B(E, X) = 1 + (b-1)X \quad \text{for } K = 1 \tag{13}$$

Table 5
Z_{eq} and G-P fitting parameters for S0 (0 PbO mol%).

Energy (MeV)	S0: 0PbO−40B_2O_3−25Na_2O−5Li_2O−30SiO_2					
	Z_{eq}	b	c	a	X_k	d
0.015	9.761	1.090	0.399	0.210	12.741	−0.108
0.02	9.803	1.206	0.437	0.194	13.942	−0.103
0.03	9.858	1.617	0.562	0.145	15.209	−0.076
0.04	9.891	2.232	0.771	0.070	15.423	−0.036
0.05	9.916	2.937	0.924	0.040	14.059	−0.031
0.06	9.938	3.401	1.118	−0.006	13.423	−0.010
0.08	9.962	3.761	1.402	−0.065	13.620	0.018
0.1	9.944	3.738	1.582	−0.094	14.191	0.031
0.15	9.757	3.449	1.761	−0.121	14.623	0.040
0.2	10.028	3.070	1.762	−0.122	14.456	0.040
0.3	8.938	2.796	1.838	−0.137	14.172	0.048
0.4	10.251	2.514	1.640	−0.110	14.891	0.034
0.5	10.477	2.369	1.575	−0.103	14.759	0.033
0.6	10.000	2.286	1.539	−0.098	15.091	0.032
0.8	10.000	2.137	1.454	−0.087	14.899	0.030
1	10.000	2.045	1.375	−0.074	15.296	0.026
1.5	9.665	1.899	1.247	−0.052	14.901	0.020
2	8.899	1.823	1.161	−0.035	15.076	0.013
3	8.912	1.673	1.057	−0.010	10.790	−0.003
4	8.950	1.618	0.991	0.005	17.803	−0.008
5	8.978	1.547	0.950	0.016	14.702	−0.015
6	8.948	1.501	0.916	0.027	14.142	−0.024
8	8.944	1.413	0.895	0.033	12.731	−0.022
10	8.946	1.354	0.873	0.040	13.709	−0.028
15	8.945	1.264	0.835	0.055	14.792	−0.045

Table 6
Z_{eq} and G-P fitting parameters for S1 (5 PbO mol%).

Energy (MeV)	S1: 5PbO−40B_2O_3−25Na_2O−5Li_2O−25SiO_2					
	Z_{eq}	b	c	a	X_k	d
0.015	12.855	1.030	0.395	0.207	15.205	−0.138
0.02	14.720	1.044	0.430	0.176	14.870	−0.085
0.03	15.422	1.130	0.391	0.214	14.186	−0.115
0.04	15.932	1.261	0.419	0.203	14.589	−0.112
0.05	16.337	1.418	0.477	0.181	14.543	−0.102
0.06	16.679	1.572	0.552	0.150	14.531	−0.084
0.08	17.219	1.823	0.696	0.097	14.586	−0.056
0.1	26.921	1.356	0.541	0.151	14.040	−0.083
0.15	28.510	1.540	0.686	0.097	14.010	−0.054
0.2	29.449	1.686	0.822	0.057	13.648	−0.039
0.3	30.665	1.823	0.979	0.016	12.809	−0.023
0.4	31.414	1.865	1.082	−0.006	12.047	−0.018
0.5	31.918	1.866	1.154	−0.024	15.731	−0.004
0.6	32.230	1.857	1.175	−0.029	20.968	−0.001
0.8	32.533	1.838	1.187	−0.033	16.247	0.000
1	32.676	1.804	1.183	−0.033	19.063	0.005
1.5	26.926	1.745	1.193	−0.039	16.689	0.011
2	17.165	1.754	1.148	−0.030	15.168	0.007
3	13.000	1.673	1.057	−0.010	10.790	−0.003
4	12.143	1.599	0.994	0.006	12.901	−0.010
5	11.799	1.538	0.944	0.022	11.145	−0.021
6	11.577	1.488	0.926	0.027	11.750	−0.021
8	11.414	1.406	0.902	0.033	13.666	−0.027
10	11.303	1.345	0.879	0.042	13.159	−0.033
15	11.243	1.260	0.829	0.062	14.322	−0.055

Table 7
Z_{eq} and G-P fitting parameters for S2 (10 PbO mol%).

Energy (MeV)	S2: 10 PbO−40B_2O_3−25Na_2O−5Li_2O-20 SiO_2					
	Z_{eq}	b	c	a	X_k	d
0.015	14.91	1.02	0.39	0.22	12.01	−0.13
0.02	17.55	1.03	0.32	0.25	20.81	−0.23
0.03	18.45	1.07	0.36	0.24	12.99	−0.13
0.04	19.07	1.15	0.38	0.22	13.93	−0.12
0.05	19.57	1.24	0.41	0.21	14.17	−0.12
0.06	19.98	1.34	0.46	0.19	14.25	−0.11
0.08	20.64	1.53	0.56	0.15	14.37	−0.08
0.1	33.13	1.24	0.43	0.21	13.84	−0.12
0.15	34.42	1.39	0.59	0.13	14.19	−0.07
0.2	36.05	1.57	0.65	0.12	14.01	−0.07
0.3	37.43	1.67	0.82	0.06	13.87	−0.04
0.4	38.22	1.76	0.95	0.02	13.49	−0.03
0.5	38.75	1.80	1.03	0.00	14.74	−0.02
0.6	39.10	1.81	1.06	0.00	15.84	−0.01
0.8	39.46	1.81	1.10	−0.01	14.56	−0.01
1	39.58	1.79	1.11	−0.02	14.76	−0.01
1.5	35.12	1.68	1.17	−0.03	12.55	0.01
2	24.23	1.71	1.14	−0.03	19.66	0.01
3	17.05	1.67	1.06	−0.01	10.79	0.00
4	15.38	1.59	1.00	0.01	13.19	−0.02
5	14.70	1.52	0.97	0.02	11.70	−0.02
6	14.30	1.47	0.95	0.02	14.15	−0.02
8	13.92	1.39	0.93	0.03	13.50	−0.03
10	13.74	1.33	0.91	0.04	13.28	−0.03
15	13.61	1.24	0.88	0.05	13.98	−0.04

Table 8
Z_{eq} and G-P fitting parameters for S2 (15 PbO mol%).

Energy (MeV)	S3: 15 PbO−40B_2O_3−25Na_2O−5Li_2O−15SiO_2					
	Z_{eq}	b	c	a	X_k	d
0.015	16.60	1.01	0.36	0.27	16.34	−0.26
0.02	19.76	1.02	0.41	0.21	11.24	−0.10
0.03	20.75	1.05	0.37	0.22	14.02	−0.15
0.04	21.44	1.11	0.36	0.24	13.43	−0.13
0.05	21.98	1.18	0.39	0.22	14.09	−0.12
0.06	22.43	1.25	0.43	0.20	14.21	−0.11
0.08	23.16	1.40	0.52	0.16	14.42	−0.09
0.1	37.64	1.20	0.36	0.25	13.79	−0.14
0.15	39.59	1.29	0.52	0.16	14.35	−0.08
0.2	40.75	1.49	0.54	0.16	14.24	−0.09
0.3	42.16	1.59	0.73	0.08	14.48	−0.04
0.4	43.01	1.69	0.88	0.04	14.17	−0.03
0.5	43.58	1.74	0.96	0.02	14.27	−0.03
0.6	43.95	1.76	1.00	0.01	13.96	−0.02
0.8	44.34	1.77	1.05	0.00	14.04	−0.01
1	44.51	1.75	1.07	−0.01	13.43	−0.01
1.5	40.77	1.63	1.17	−0.03	5.90	0.00
2	30.52	1.68	1.13	−0.02	23.41	0.00
3	21.18	1.64	1.07	−0.01	12.97	−0.01
4	18.68	1.58	1.01	0.01	11.35	−0.02
5	17.65	1.51	0.98	0.01	13.19	−0.02
6	17.08	1.46	0.96	0.02	13.59	−0.02
8	16.47	1.39	0.93	0.03	13.42	−0.03
10	16.22	1.32	0.92	0.04	13.69	−0.03
15	16.01	1.23	0.90	0.05	13.24	−0.05

$$K(E,\ X) = cX^a + d\frac{\tanh\left(\frac{X}{X_K} - 2\right) - \tanh(-2)}{1 - \tanh(-2)} \quad (14)$$

where X is the distance between the source and the detector in terms of mfp, B is the value of the EBF at 1 mfp, K (E, X) is the dose multiplicative factor, and b, c, a, X_K, and d are the computed G-P fitting parameters, which depend on the attenuating medium and source energy. The G-P fitting parameters (b, c, a, X_k, and d) for the prepared glasses in the gamma ray energy range from 0.015 to 15 MeV up to 40 mfp were logarithmically interpolated using the following formula, which is similar to Equation (11) [32,33]:

$$P = \frac{P_1(\log Z_2 - \log Z_{eq}) + P_2(\log Z_{eq} - \log Z_1)}{\log Z_2 - \log Z_1} \quad (15)$$

where P_1 and P_2 are the values of the G-P fitting parameters corresponding to the atomic numbers Z_1 and Z_2 at a given energy, respectively. The G-P fitting parameters for the elements were obtained from a report by the American Nuclear Society [34].

The fast neutron removal cross section for any material is the

Table 9
Z_{eq} and G-P fitting parameters for S4 (20 PbO mol%).

Energy (MeV)	S4: 20PbO−40B_2O_3−25Na_2O−5Li_2O−10SiO_2					
	Z_{eq}	b	c	a	X_k	d
0.015	18.000	1.009	0.495	0.141	29.380	−0.285
0.02	21.657	1.015	0.347	0.314	11.042	−0.246
0.03	22.702	1.043	0.373	0.209	20.127	−0.214
0.04	23.432	1.086	0.347	0.242	12.609	−0.125
0.05	24.000	1.138	0.378	0.226	14.050	−0.130
0.06	24.476	1.191	0.417	0.204	14.188	−0.113
0.08	25.232	1.301	0.482	0.176	14.465	−0.095
0.1	41.360	1.163	0.309	0.285	13.756	−0.153
0.15	43.383	1.237	0.460	0.194	14.333	−0.102
0.2	44.564	1.402	0.509	0.172	14.402	−0.097
0.3	46.002	1.493	0.688	0.094	14.354	−0.047
0.4	46.842	1.598	0.827	0.055	14.155	−0.039
0.5	47.433	1.659	0.903	0.035	14.142	−0.032
0.6	47.824	1.684	0.958	0.019	14.000	−0.023
0.8	48.223	1.708	1.014	0.005	14.075	−0.017
1	48.389	1.704	1.041	−0.002	13.430	−0.015
1.5	45.166	1.601	1.145	−0.026	10.119	−0.001
2	35.739	1.642	1.127	−0.022	17.790	−0.002
3	25.114	1.629	1.060	−0.006	12.155	−0.012
4	21.957	1.567	1.015	0.006	12.363	−0.018
5	20.625	1.505	0.986	0.015	13.199	−0.023
6	19.862	1.460	0.961	0.023	13.221	−0.030
8	19.127	1.381	0.933	0.034	13.477	−0.039
10	18.775	1.317	0.925	0.038	13.506	−0.042
15	18.493	1.231	0.881	0.060	13.675	−0.061

Table 10
Z_{eq} and G-P fitting parameters for S4 (25 PbO mol%).

Energy (MeV)	S5: 25PbO−40B_2O_3−25Na_2O−5Li_2O−5SiO_2					
	Z_{eq}	b	c	a	X_k	d
0.015	19.408	1.011	0.149	0.558	13.004	−0.542
0.02	23.338	1.014	0.258	0.439	11.184	−0.397
0.03	24.421	1.035	0.374	0.199	25.085	−0.270
0.04	25.174	1.067	0.339	0.246	11.948	−0.121
0.05	25.771	1.103	0.367	0.231	14.014	−0.135
0.06	26.257	1.144	0.401	0.211	14.113	−0.116
0.08	27.040	1.239	0.461	0.184	14.297	−0.102
0.1	44.593	1.240	0.216	0.427	13.764	−0.213
0.15	46.664	1.228	0.391	0.237	14.136	−0.130
0.2	47.856	1.315	0.504	0.172	14.537	−0.094
0.3	49.312	1.420	0.654	0.104	14.251	−0.050
0.4	50.190	1.528	0.786	0.066	14.139	−0.043
0.5	50.722	1.597	0.864	0.045	14.064	−0.036
0.6	51.083	1.627	0.924	0.027	13.986	−0.026
0.8	51.490	1.662	0.984	0.011	13.994	−0.019
1	51.657	1.664	1.015	0.004	13.383	−0.018
1.5	48.869	1.577	1.127	−0.022	13.359	−0.004
2	40.268	1.612	1.127	−0.021	13.969	−0.004
3	29.026	1.617	1.059	−0.004	12.212	−0.015
4	25.335	1.555	1.024	0.005	12.843	−0.019
5	23.672	1.492	1.000	0.013	13.152	−0.025
6	22.802	1.451	0.971	0.023	13.280	−0.033
8	21.795	1.369	0.953	0.030	13.563	−0.038
10	21.406	1.309	0.938	0.038	13.696	−0.046
15	21.059	1.215	0.924	0.050	14.000	−0.056

probability of a fast neutron being removed from a group of penetrative uncollided neutrons after the first collision with the material target. The effective removal cross section is approximately constant in the neutron energy range of 2–12 MeV [32]. In the case of a mixture of elements, the removal cross section is calculated using the following formula:

$$\Sigma_R = \sum_i w_i (\Sigma_R)_i \tag{16}$$

where $(\Sigma_R)_i$ and w_i are the elemental removal cross section and the weight percentage, respectively, for the ith element of the mixture.

4. Results and discussion

4.1. Powder XRD analysis

The XRD patterns obtained for the prepared glasses are shown in Fig. 1. The lack of sharp peaks indicates the randomness (or amorphicity) of the structure of the prepared glasses, which was further supported by the increases in the molar volume values, as described later.

4.2. FTIR spectra

The FTIR absorption spectra obtained for the prepared glasses are shown in Fig. 2. Lead atoms that entered the glass network as a former led to Pb−*O*−B vibrations or Pb−*O*−Si bending bonds. The major absorption bands were clearly observed around 472, 711, 968, and 1385 cm^{-1}, and the designations of these bands are summarized in Table 1. Some minor differences in the band intensities and peak positions were also observed. The PbO doped and undoped glasses obtained the same FTIR spectra with no changes in the numbers and positions of the infrared vibrational bonds.

The narrowing of a line width indicate that strain/distortion associated with the borosilicate network is reduced, which normally occurs when bridging oxygen atoms are converted into non-bridging oxygen (NBO) atoms. Thus, that incorporation of PbO at the expense of SiO_2 creates more NBO atoms in glass. The NBO atoms can be created via the formation of Si−*O*−Pb/B−*O*−Pb from Si−*O*−Si/B−*O*−B/Si−*O*−B bonds. We observed that the intensity of the BO_3 band increased gradually as the PbO content increased and the maximum value was reached at 25 mol% PbO, thereby confirming the formation of NBO atoms in the glass network.

4.3. Chemical composition, mass density, and molar volume

The chemical compositions (mol%) of the prepared glasses at different PbO mol% are illustrated in Table 2. The mass densities and molar volumes of the glasses are shown in Fig. 3. These results indicate that the increase in the mass density was due to the higher molecular weight of PbO compared with the other constituents. As the PbO mol% increased, the Pb^{+2} ions occupied the network and the amount of former positions increased, and thus the NBOs increased in the network to randomize the structure. The molar volume decreased as a consequence.

4.4. Gamma ray shielding properties

The Z_{eff} values for all of the prepared glasses in the energy range from 0.015 to 15 MeV are shown in Fig. 4. All of the prepared glasses containing PbO exhibited similar behavior. The attenuation cross-section is proportional to Z^{4-5} for photoelectric attenuation, proportional to Z for a Compton interaction, and proportional to Z^2 for pair production. Therefore, the Z_{eff} values increased as the percentage of PbO increased. The increase in Z_{eff} with the addition of PbO was attributed to the replacement of SiO_2 with PbO because the cross section of PbO is larger than that of SiO_2. In the low energy range $\leq$0.1 MeV where photoelectric interactions are dominant, all of the samples exhibited an evident increase in Z_{eff} as the incident photon energy increased. The highest Z_{eff} value in all of the samples was observed at about 0.1 MeV, probably because one of the Pb absorption edges (K-edge) occurred at 0.088 MeV [25]. A rapid decrease in the Z_{eff} value was detected in the energy range from 0.1 to 1 MeV, where photoelectric absorption decreased and Compton scattering gradually became the dominating interaction, and the probability of interaction was inversely proportional to the energy. In the range from 1 to 15 MeV, pair production interaction was dominant and the probability of interaction was directly proportional to the energy.

The mass attenuation coefficients for the prepared glass samples

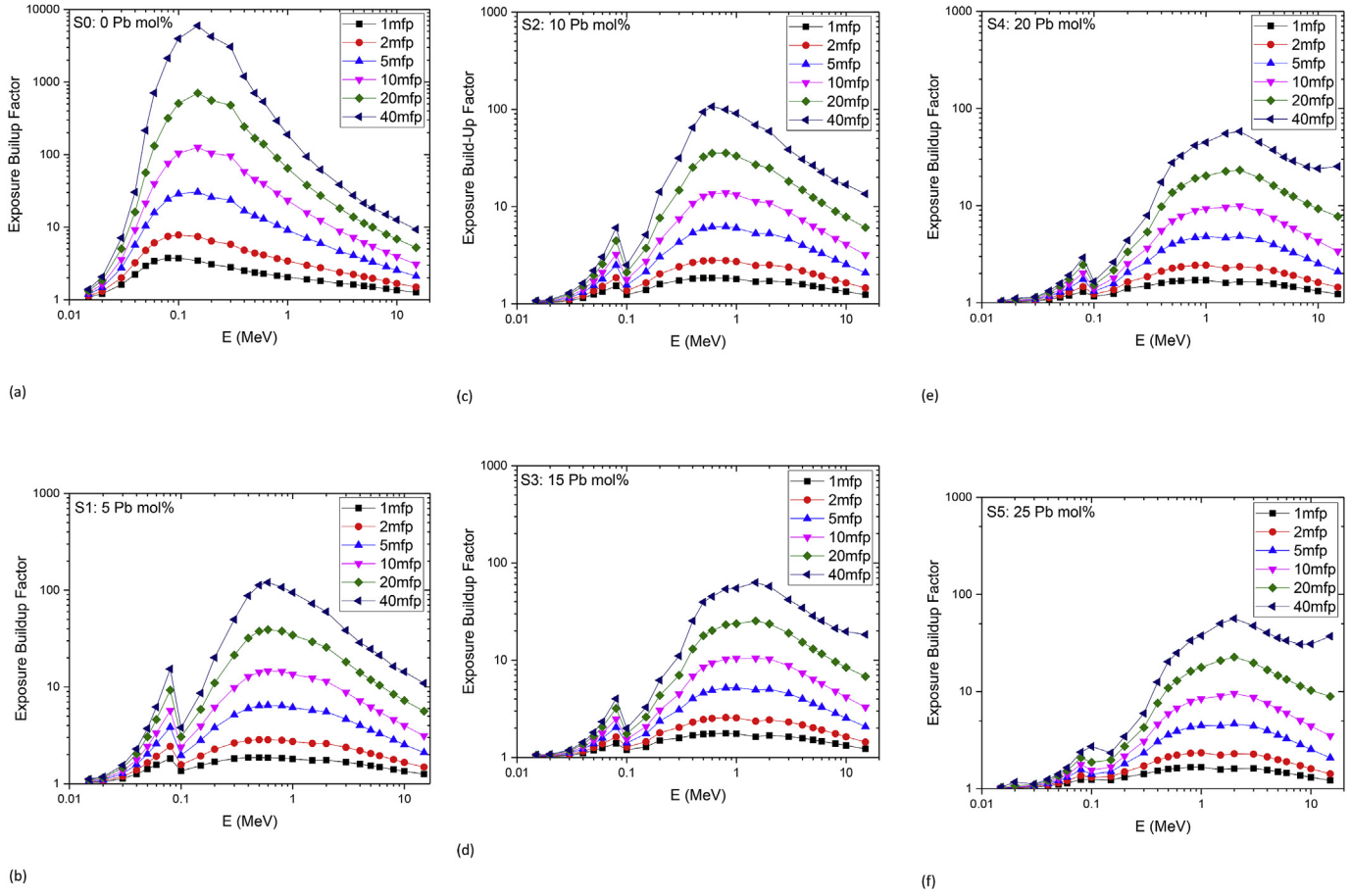

Fig. 7. Exposure build-up factors for lithium sodium borosilicate glasses containing PbO at photon energies of 0.015–15 MeV up to 40 mfp for: (a) zero PbO mol%, (b) 5 PbO mol%, (c) 10 PbO mol%, (d) 15 PbO mol%, (e) 20 PbO mol%, and (f) 25 PbO mol%.

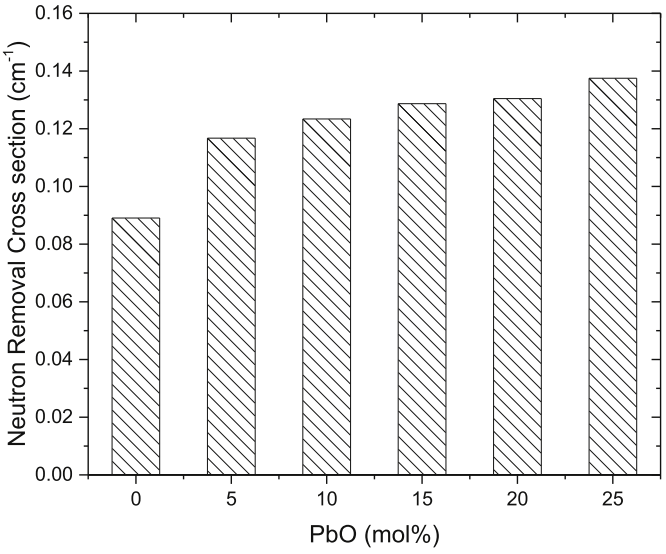

Fig. 8. Fast neutron removal cross sections for lithium sodium borosilicate glasses containing PbO.

compared with Portland concrete are shown in Fig. 5. The results indicated that as the weight fraction of PbO increased, there were obvious increases in the mass attenuation coefficients of the prepared glasses. All of the prepared glasses (except S0) had higher mass attenuation coefficients than Portland concrete. This behavior can be attributed to the increase in the atomic number increasing the probability of gamma ray interactions with the prepared glasses. As shown in Fig. 6, the HVL values obtained for all of the glass samples increased with the photon energy. Thus, the variations in the Z_{eff} values for the prepared glasses with differences in PbO mol% and the photon energy were direct consequences of the mass attenuation results and the corresponding HVL values. As shown in Table 4, the mass attenuation coefficients and Z_{eff} values were comparable at the same lead concentration and gamma ray energy for barite concrete, Portland concrete, and the glasses doped with Pb. According to Table 3, all of the prepared glass samples achieved better gamma attenuation than barite and Portland concrete. The significantly low HVL result at 25 PbO mol% compared with the other glass samples at all energy values suggests that this glass composition may be used in various gamma ray shielding applications.

In order to validate the theoretically calculated shielding parameters, the measured and calculated values of the mass attenuation coefficient, HVL, Z_{eff}, and N_{eff} at 0.239, 0.662, 0.911, and 1.332 MeV are shown in Table 4 for all of the prepared glasses. The values were within 5% of the theoretical values for all of the parameters.

The G-P fitting parameters for the S0−S5 samples are shown in Tables 5–10 and the corresponding EBFs are shown in Fig. 7(a–f).

The EBF results can interpreted based on their dependences on the photon energy, PbO mol%, and penetration depth.

As shown in Fig. 7(a–f), the minimum EBF values occurred in the low and high energy regions, and the values were higher in the intermediate energy region at all PbO concentrations. It is likely that the photoelectric effect and pair production led to complete absorption in the low and high energy regions, respectively. By contrast, the intermediate region was distinguished by multiple Compton scattering, and thus higher EBF values [48]. The observed peak in the EBF values for all

of the glasses at 0.088 MeV was attributed to the absorption K-edge of Pb.

The penetration depth is inversely proportional to the attenuation coefficient, and the attenuation coefficient is directly proportional to the PbO mol%. Therefore, the penetration depth is inversely proportional to the PbO mol%. Multiple scattering events occur at large penetration depths, so we inferred that either increasing the penetration depth or decreasing the PbO mol% caused the increase in the EBF values, as shown in Fig. 7(a–f).

4.5. Fast neutron removal cross section

The fast neutron removal cross-section Σ_R (cm^{-1}) values calculated for the prepared glasses are shown in Fig. 8. The lowest Σ_R value was obtained at 0 mol% PbO and the highest at 25 mol% PbO. These results indicate that the composite glass with the highest amount of the heavy element had the highest neutron removal cross section. Thus, low-Z elements may be responsible for neutron removal [49] but a combination of both low-Z and high-Z elements could achieve similar results.

5. Conclusions

In this study, several lead sodium lithium borosilicate glasses were prepared and studied to assess their possible uses as transparent radiation shielding materials. The mass attenuation coefficient (μ_m), Z_{eff}, and N_{eff} values increased as the amount of PbO mol% increased and decreased as the photon energy increased. The EBF values were calculated for the Pb borosilicate glasses at photon energies in the range of 0.015–15 MeV with a penetration depth up to 40 mfp and at different values of PbO mol%. The neutron attenuation capacities of the prepared glasses were determined by calculating the fast neutron removal cross sections using the partial density method. The experimental and theoretical results agree within 5% for the mass attenuation coefficient, HVL, Z_{eff}, and N_{eff} values for all of the prepared glasses at 0.239, 0.662, 0.911, and 1.332 MeV. According to the volume required for shield design and the mass attenuation coefficient values, the glasses prepared in this study have the advantages of being transparent to visible light and providing better radiation shielding compared with other materials such as barite concrete.

References

[1] K.J. Singh, N. Singh, R.S. Kaundal, K. Singh, Gamma-ray shielding and structural properties of PbO-SiO2 glasses, Nucl. Instrum. Methods Phys. Res. Sect. B Beam Interact. Mater. Atoms 266 (2008) 944–948, https://doi.org/10.1016/j.nimb.2008.02.004.

[2] S.R. Manohara, S.M. Hanagodimath, L. Gerward, Photon interaction and energy absorption in glass: a transparent gamma ray shield, J. Nucl. Mater. 393 (2009) 465–472, https://doi.org/10.1016/j.jnucmat.2009.07.001.

[3] M.I. Sayyed, M. Çelikbilek Ersundu, A.E. Ersundu, G. Lakshminarayana, P. Kostka, Investigation of radiation shielding properties for MeO-PbCl2-TeO2(MeO = Bi2O3, MoO3, Sb2O3, WO3, ZnO) glasses, Radiat. Phys. Chem. 144 (2018) 419–425, https://doi.org/10.1016/j.radphyschem.2017.10.005.

[4] A. Kumar, Gamma ray shielding properties of PbO-Li 2 O-B 2 O 3 glasses, Radiat. Phys. Chem. 136 (2017) 50–53, https://doi.org/10.1016/j.radphyschem.2017.03.023.

[5] M. Kurudirek, Y. Özdemir, Ö. Imek, R. Durak, Comparison of some lead and non-lead based glass systems, standard shielding concretes and commercial window glasses in terms of shielding parameters in the energy region of 1 keV-100 GeV: a comparative study, J. Nucl. Mater. 407 (2010) 110–115, https://doi.org/10.1016/j.jnucmat.2010.10.007.

[6] R. Kaur, S. Singh, O.P. Pandey, Absorption spectroscopic studies on gamma irradiated bismuth borosilicate glasses, J. Mol. Struct. 1049 (2013) 386–391, https://doi.org/10.1016/j.molstruc.2013.06.056.

[7] R. Kaur, S. Singh, O.P. Pandey, FTIR structural investigation of gamma irradiated BaO-Na 2O-B 2O 3-SiO 2 glasses, Phys. B Condens. Matter 407 (2012) 4765–4769, https://doi.org/10.1016/j.physb.2012.08.031.

[8] R. Kaur, S. Singh, O.P. Pandey, Influence of CdO and gamma irradiation on the infrared absorption spectra of borosilicate glass, J. Mol. Struct. 1049 (2013) 409–413, https://doi.org/10.1016/j.molstruc.2013.06.072.

[9] P. Limkitjaroenporn, J. Kaewkhao, P. Limsuwan, W. Chewpraditkul, Physical, optical, structural and gamma-ray shielding properties of lead sodium borate glasses, J. Phys. Chem. Solids 72 (2011) 245–251, https://doi.org/10.1016/j.jpcs.2011.01.007.

[10] M. Kurudirek, Heavy metal borate glasses: potential use for radiation shielding, J. Alloy. Comp. 727 (2017) 1227–1236, https://doi.org/10.1016/j.jallcom.2017.08.237.

[11] M.I. Sayyed, Bismuth modified shielding properties of zinc boro-tellurite glasses, J. Alloy. Comp. 688 (2016) 111–117, https://doi.org/10.1016/j.jallcom.2016.07.153.

[12] D.K. Gaikwad, M.I. Sayyed, S.S. Obaid, S.A.M. Issa, P.P. Pawar, Gamma ray shielding properties of TeO2-ZnF2-As2O3-Sm2O3glasses, J. Alloy. Comp. 765 (2018) 451–458, https://doi.org/10.1016/j.jallcom.2018.06.240.

[13] P. Kaur, K.J. Singh, S. Thakur, Evaluation of the gamma radiation shielding parameters of bismuth modified quaternary glass system, AIP Conf. Proc, 2018, https://doi.org/10.1063/1.5032878.

[14] A.E. Ersundu, M. Büyükyıldız, M. Çelikbilek Ersundu, E. Şakar, M. Kurudirek, The heavy metal oxide glasses within the WO3-MoO3-TeO2system to investigate the shielding properties of radiation applications, Prog. Nucl. Energy 104 (2018) 280–287, https://doi.org/10.1016/j.pnucene.2017.10.008.

[15] A.E. Ersundu, M. Çelikbilek, S. Aydin, Characterization of B 2O 3 and/or WO 3 containing tellurite glasses, J. Non-Cryst. Solids 358 (2012) 641–647, https://doi.org/10.1016/j.jnoncrysol.2011.11.012.

[16] B.O. El-bashir, M.I. Sayyed, M.H.M. Zaid, K.A. Matori, Comprehensive study on physical, elastic and shielding properties of ternary BaO-Bi2O3-P2O5glasses as a potent radiation shielding material, J. Non-Cryst. Solids 468 (2017) 92–99, https://doi.org/10.1016/j.jnoncrysol.2017.04.031.

[17] R. El-Mallawany, M.I. Sayyed, M.G. Dong, Comparative shielding properties of some tellurite glasses: Part 2, J. Non-Cryst. Solids 474 (2017) 16–23, https://doi.org/10.1016/j.jnoncrysol.2017.08.011.

[18] S. Ibrahim, M.M. Gomaa, H. Darwish, Influence of Fe2O3 on the physical, structural and electrical properties of sodium lead borate glasses, J. Adv. Ceram. 3 (2014) 155–164, https://doi.org/10.1007/s40145-014-0107-z.

[19] T.Q. Leow, P.M. Leong, T.Y. Eeu, Z. Ibrahim, R. Hussin, Study of Structural and luminescence properties of lead lithium borophosphate glass system doped with ti ions, Sains Malays. 43 (2014) 929–934.

[20] M. Abdel-Baki, A.M. Salem, F.A. Abdel-Wahab, F. El-Diasty, Bond character, optical properties and ionic conductivity of Li2O/B2O3/SiO2/Al2O3 glass: effect of structural substitution of Li2O for LiCl, J. Non-Cryst. Solids 354 (2008) 4527–4533, https://doi.org/10.1016/j.jnoncrysol.2008.07.003.

[21] R. Kaur, S. Singh, O.P. Pandey, Structural variation in gamma ray irradiated PbO–Na2O–B2O3–SiO2 glasses, Solid State Commun. 188 (2014) 40–44, https://doi.org/10.1016/j.ssc.2014.02.022.

[22] S.Y. Marzouk, R. Seoudi, D.A. Said, M.S. Mabrouk, Linear and non-linear optics and FTIR characteristics of borosilicate glasses doped with gadolinium ions, Opt. Mater. 35 (2013) 2077–2084, https://doi.org/10.1016/j.optmat.2013.05.023.

[23] C. Bootjomchai, J. Laopaiboon, C. Yenchai, R. Laopaiboon, Gamma-ray shielding and structural properties of barium-bismuth-borosilicate glasses, Radiat. Phys. Chem. 81 (2012) 785–790, https://doi.org/10.1016/j.radphyschem.2012.01.049.

[24] V.P. Singh, N.M. Badiger, J. Kaewkhao, Radiation shielding competence of silicate and borate heavy metal oxide glasses: comparative study, J. Non-Cryst. Solids 404 (2014) 167–173, https://doi.org/10.1016/j.jnoncrysol.2014.08.003.

[25] M.J. Berger, J.H. Hubbell, S.M. Seltzer, J. Chang, J.S. Coursey, R. Sukumar, D.S. Zucker, K. Olsen, XCOM: Photon Cross Sections Database, NIST Standard Reference Database 8 (XGAM), (2010) NBSIR 87-3597.

[26] S.A. Tijani, S.M. Kamal, Y. Al-Hadeethi, M. Arib, M.A. Hussein, S. Wageh, L.A. Dim, Radiation shielding properties of transparent erbium zinc tellurite glass system determined at medical diagnostic energies, J. Alloy. Comp. 741 (2018) 293–299, https://doi.org/10.1016/j.jallcom.2018.01.109.

[27] M.L. Taylor, R.L. Smith, F. Dossing, R.D. Franich, Robust calculation of effective atomic numbers: the Auto-Zeff software, Med. Phys. Med. Phys. Med. Phys. Med. Phys.Marie Sklodowska-Curie Med. Phys. 391 (2012), https://doi.org/10.1118/1.3689810 1769–2491.

[28] B.T. Tonguc, H. Arslan, M.S. Al-Buriahi, Studies on mass attenuation coefficients, effective atomic numbers and electron densities for some biomolecules, Radiat. Phys. Chem. 153 (2018) 86–91, https://doi.org/10.1016/j.radphyschem.2018.08.025.

[29] P. Sathiyaraj, E.J.J. Samuel, C.C.S. Valeriano, M. Kurudirek, Effective atomic number and buildup factor calculations for metal nano particle doped polymer gel, Vacuum 143 (2017) 138–149, https://doi.org/10.1016/j.vacuum.2017.06.005.

[30] Y. Harima, An historical review and current status of buildup factor calculations and applications, Radiat. Phys. Chem. 41 (1993) 631–672, https://doi.org/10.1016/0969-806X(93)90317-N.

[31] E. Kavaz, N.Y. Yorgun, Gamma ray buildup factors of lithium borate glasses doped with minerals, J. Alloy. Comp. 752 (2018) 61–67, https://doi.org/10.1016/j.jallcom.2018.04.106.

[32] M.F. Kaplan, Concrete Radiation Shielding : Nuclear Physics, Concrete Properties, Design and Construction, Longman Scientific & Technical, 1989, https://inis.iaea.org/search/search.aspx?orig_q=RN:22004467 , Accessed date: 13 July 2018.

[33] V.P. Singh, N.M. Badiger, Gamma ray and neutron shielding properties of some alloy materials, Ann. Nucl. Energy 64 (2014) 301–310, https://doi.org/10.1016/j.anucene.2013.10.003.

[34] ANSI/ANS-6.4.3, Gamma-Ray Attenuation Coefficients and Buildup Factors for Engineering Materials, American Nuclear Society, La Grange Park, 1991.

[35] D. Shajan, P. Murugasen, S. Sagadevan, Analysis on the structural, spectroscopic, and dielectric properties of borate glass, Dig. J. Nanomater. Biostruct. 11 (2016) 177–183.

[36] I.S. Mustafa, H.M. Kamari, W.M.D. Wan Yusoff, S.A. Aziz, A.A. Rahman, Structural and optical properties of lead-boro-tellurrite glasses induced by Gamma-ray, Int. J. Mol. Sci. 14 (2013) 3201–3214, https://doi.org/10.3390/ijms14023201.

[37] A.K. Yadav, C.R. Gautam, Structural and optical studies of Fe_2O_3 doped barium strontium titanate borosilicate glasses, Indian J. Pure Appl. Phys. 53 (2015).
[38] S. Rani, S. Sanghi, A. Agarwal, V.P. Seth, Study of optical band gap and FTIR spectroscopy of Li2O??Bi2O3??P2O5 glasses, Spectrochim. Acta Part A Mol. Biomol. Spectrosc. 74 (2009) 673–677, https://doi.org/10.1016/j.saa.2009.07.023.
[39] C. Gautam, A.K. Yadav, V. Kumar Mishra, K. Vikram, Synthesis, IR and Raman spectroscopic studies of (Ba,Sr)TiO 3 borosilicate glasses with addition of La 2 O 3, Open J. Inorg. Non-Metallic Mater. 2 (2012) 47–54, https://doi.org/10.4236/ojinm.2012.24005.
[40] C.R. Gautam, D. Kumar, O. Parkash, IR study of Pb-Sr titanate borosilicate glasses, Bull. Mater. Sci. 33 (2010) 145–148, https://doi.org/10.1007/s12034-010-0020-1.
[41] A.K. Mandal, D. Agrawal, R. Sen, Preparation of homogeneous barium borosilicate glass using microwave energy, J. Non-Cryst. Solids (2013) 371–372, https://doi.org/10.1016/j.jnoncrysol.2013.04.044 41–46.
[42] Khairy M. Tohamy, Islam E. Soliman, Asem E. Motawea, Mohamed A. Aboelnasr, Characterization and bioactive study of borosilicate sol-gel glass, Nat. Sci. 13 (8) (2015) 145–154.
[43] K. Kirdsiri, J. Kaewkhao, A. Pokaipisit, W. Chewpraditkul, P. Limsuwan, Gamma-rays shielding properties of xPbO:(100 − x)B2O3 glasses system at 662keV, Ann. Nucl. Energy 36 (2009) 1360–1365, https://doi.org/10.1016/j.anucene.2009.06.019.
[44] M.H. Kharita, R. Jabra, S. Yousef, T. Samaan, Shielding properties of lead and barium phosphate glasses, Radiat. Phys. Chem. 81 (2012) 1568–1571, https://doi.org/10.1016/j.radphyschem.2012.05.002.
[45] K. Kaur, K.J. Singh, V. Anand, Correlation of gamma ray shielding and structural properties of PbO-BaO-P2O5 glass system, Nucl. Eng. Des. 285 (2015) 31–38, https://doi.org/10.1016/j.nucengdes.2014.12.033.
[46] R. Picha, J. Channuie, S. Khaweerat, T. Liamsuwan, J. Promping, W. Ratanatongchai, K. Silva, S. Wonglee, Gamma and neutron attenuation properties of barite-cement mixture, J. Phys. Conf. Ser, 2015, https://doi.org/10.1088/1742-6596/611/1/012002.
[47] I. Akkurt, H. Akyildirim, F. Karipçin, B. Mavi, Chemical corrosion on gamma-ray attenuation properties of barite concrete, J. Saudi Chem. Soc. 16 (2012) 199–202, https://doi.org/10.1016/j.jscs.2011.01.003.
[48] M.I. Sayyed, G. Lakshminarayana, I.V. Kityk, M.A. Mahdi, Evaluation of shielding parameters for heavy metal fluoride based tellurite-rich glasses for gamma ray shielding applications, Radiat. Phys. Chem. 139 (2017) 33–39, https://doi.org/10.1016/j.radphyschem.2017.05.013.
[49] M.A. Ashraff Rosdi, P.S. Goh, F. Idris, S. Shalbi, M.S. Sarkawi, N.S. Mohd Ali, N.L. Jamsari, A.S. Ramli, A. Azman, Neutron and gamma ray fluences measurement at radial Beam Port 1 of TRIGA MARK II PUSPATI research reactor, IOP Conf. Ser. Mater. Sci. Eng. 2018, https://doi.org/10.1088/1757-899X/298/1/012033.